Environmental Earth Sciences (2021) 80:616
https://doi.org/10.1007/s12665-021-09916-9

ORIGINAL ARTICLE

Influence of natural discontinuities and mechanical properties on the fragmentation of marble by blasting in Central Africa

Michel Constant Njock[1] · Jorelle Larissa Meli'i[1] · Yvonne Koffi Poufonne[2] · Ibrahim Ngapouth Mbouombouo[1] · Tamto Have Linda Well[1] · Zakari Arétouyap[3] · Eliézer Manguelle-Dicoum[1,4] · Philippe Njandjock Nouck[1,5]

Received: 14 March 2021 / Accepted: 27 August 2021 / Published online: 3 September 2021

Abstract

Natural discontinuities as well as mechanical properties are the difficult-to-control parameters that significantly influence the fragmentation of marble after blasting. In Central Africa, the Bidzar quarry is the only one producing marble, plagued for decades by block fragmentation problems, requiring multiple blasts that cause huge costs and environmental problems. The objective of this study is to predict the fragmentation of the Bidzar rock quarry and to improve its geological and mechanical knowledge using the Kuz–Ram method. Thus, blastability as a function of the dip of the discontinuity planes as well as fragmentation as a function of the powder factor, compressive strength and drilling mesh were studied. The results obtained show that, the rock quarry is heterogeneous, consisting mainly of fissured marble of medium hardness. Its dip is about 85°, its rock factor is 10.455 and it is class III, with a difficult blastability of 0.2654 kg/m^3. The marble from the Bidzar quarry is of excellent quality with an RQD of 93%.The fractures and discontinuity planes are spaced and of class ES2. The density of the fractures and discontinuity planes is low and of class ID2.The rock quarry is intercepted by a network of discontinuity planes marked by three families of direction, major (N30–40E, N40–50E, N160–170E), secondary (N10–20E, N50–60E, N80–90E, N140–150E, N150–160E, N170–180E) and minority (N00–10E, N20–30E, N40–50E, N70–80E, N100–110E, N110–120E, N120–130E, N130–140E). Finally, the variation in fragmentation intensity is caused by differences in the dips of the blasting planes, their compressive strength, and the variation in the drilling mesh.

Keywords Natural discontinuity · Mechanical property · Blasting · Fragmentation · Kuz–Ram model · Marble quarry

Introduction

Fragmentation of boulders by blasting has always been an important aspect in mining and is the subject of many studies (Cho and Katsuhiko 2004; Gheibie et al. 2009; Huang et al. 2020; Shaib et al. 2020; Salmi and Sellers 2021; Yusong et al. 2021). The size of the fragments obtained should also not exceed the opening of the crushing plant for efficient operation (Ebrahimi et al. 2015; Jug et al. 2017; Mohammad et al. 2019; Shaib et al. 2020; Zhendong et al. 2020). The presence of large blocks requires secondary fragmentation to further reduce the material blasting to acceptable sizes, thus increasing production costs, time losses and environmental destructive effects (De Lile 2012; Yahyaoui et al. 2018). In general, when blasting, there is not always a match between the size of the blasted blocks and the crusher mesh. In addition, knowledge of rock matrix is important in modelling a blast. These properties (natural discontinuities and physico–mechanical characteristics) are fundamental for the optimization of fragmentation and constitute the difficult-to-control parameters of a blast (Cruise 2011; Akbari et al. 2015; Jug et al. 2017). Regarding the influence of geological discontinuities on fragmentation, Hustrulid (1999) cited Burkle (1979) on the fact that, blasting results are affected by the orientation of the rock mass structures considering

✉ Philippe Njandjock Nouck
pnnouck@yahoo.com

1 Department of Physics, University of Yaounde I, Yaounde, Cameroon

2 Department of Cartography, National Institute of Cartography, Yaounde, Cameroon

3 Department of Geosciences, University of Dschang, Dschang, Cameroon

4 Department of Geotechnics, Cameroon Academy of Science, Yaounde, Cameroon

5 Ngoa-Ekelle, 812, Yaounde, Cameroon

then: dip blasting, counter dip blasting and blasting along the dip direction. Blasting on slopes oriented perpendicular to the direction of the main joints gives better fragmentation with smaller rock fragments (Belland 1968; Ash 1973). The discontinuities that are studied in the Bidzar marble quarry are of natural origin, acquired during the varied volcano-sedimentary phenomenon that prevailed in the area (Wouatong et al. 2017). These discontinuities are indeed, the layers and fracture planes in a subvertical to vertical plane, which may correspond to the blasting planes. This work aims to enhance the geological and mechanical information about the said quarry and to estimate the marble block fragments distribution that can pass to the crusher, considering the effect of natural discontinuities and mechanical properties, using the viable and generally used Kuz–Ram prediction model.

Materials

Study area and in situ *measurements*

The Bidzar quarry is a marble deposit located in Central Africa between Nigeria, Chad, Central African Republic and Cameroon. This marble is used not only in the manufacture of cement but also in decoration. The annual production of the quarry varies between 250,000 and 1,100,000 tons per year. This quarry is located at the geographical coordinates 09°55' and 09°56' North longitude, 14°07′13" and 14°07′68" East latitude (Fig. 1), and is situated in the North Cameroon Region, in the locality of Bidzar, on a hill with an average altitude of 450 m (Wouatong et al. 2017). The Bidzar rock quarry is a metamorphic type deposit. This marble alternates in some places with schist layers in a vertical dip and is sometimes adjacent to dolomite, talc, granite and gneiss. Generally, there are three varieties of marble in the quarry, white, pink and black marbles. However, white marble is in the majority. The marble and shale layers in this quarry have a major northward direction and are subvertically to vertically dipping. Joints, fractures, folds and lineations are easily observed. Indeed, this marble deposit originates from a varied volcano-sedimentary phenomenon that prevailed in the Bidzar area and whose main tectonic footprint is the D_2 deformation phase, characterized by high-grade metamorphism that led to the transformation of clays to shale, limestone to marble and quartzite sandstone to greenschist (Wouatong et al. 2017). The tectonic history of the area is characterized by two deformation phases that developed during the Neoproterozoic (Ndjeng 1998). The D_1 deformation phase which is globally NNE–SSW to N–S and the D_2 deformation phase considered as the major deformation phase, is globally NE–SW subvertically dipping. These two deformation phases are responsible for the multiple fractures that exist in the Bidzar area and its surroundings giving several fracture directions N–S, NE–SW, NNE–SSW, ENE–WSW, ESE–WNW, and NNW–SSE (Ndjeng 1998). The physical and mechanical properties of Bidzar marble measured in the field are given as follows: absolute density 2.77 kg/L, bulk density 2.75 kg/L, mechanical fragmentation strength 31–32%, wear strength 25 and 33% for grain size classes 6/10 mm and 10/14 mm, respectively, simple compressive strength is 75 MPa and indirect tensile strength 8.9 MPa (Wouatong et al. 2017).

Fifty-nine planes of natural discontinuities were measured. The direction and dip data of each plane were taken in situ at the free face using the clinometer compass. Seven major discontinuity planes, N80E60, N20E70, N56E75, N156E82, N40E85, N08E86, and N120E90, are measured and used to predict fragmentation. These natural discontinuity planes are considered as blasting planes. Each blasting plane corresponds to a direction, dip, free blasting face and a specific blast platform where the rock samples are taken (Fig. 2). Measurements of the compressive strength of the blasting planes are carried out by taking rock core sample from the platform along the direction of blasting plane and

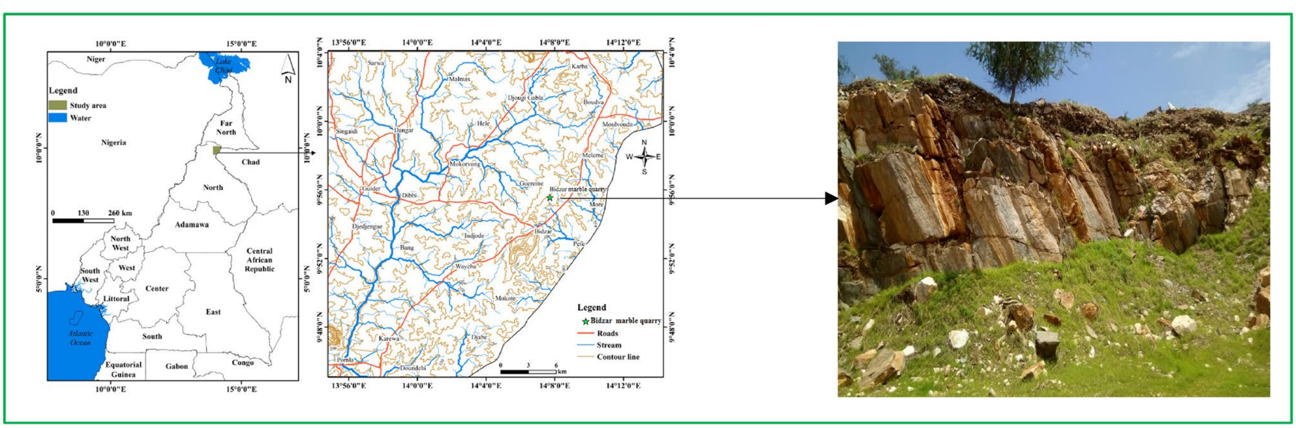

Fig. 1 Location and the geomorphological maps of the study area

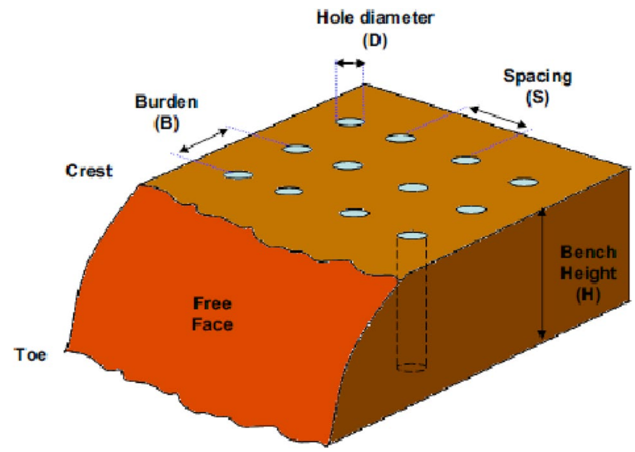

Fig. 2 Free face, platform and geometric parameters of blasting (Segaetsho 2017)

carrying out compression test on each sample in the laboratory. Five rock samples along the direction of blasting plane on the platform were taken. The distance between the points to be sampled is of 100 m and the average compressive strengths of the samples were calculated. The average compressive strengths corresponding to the 60°,70°,75°, 82°,85°,86°, and 90° dip blasting planes are 94.7 Mpa, 86.8 Mpa, 82.8 Mpa, 76.2 Mpa, 75 Mpa, 74 Mpa, and 71 Mpa, respectively. The hardness of the said planes is a function of their compressive strength (Table 1). Two types of explosives were used in the Bidzar quarry: the Explus TSR type cartridge and the Anfo type bulk explosive. The type of blasting used was electric and the meshes used in the quarry were square: 3 × 3 m, 4 × 4 m, 4.5 × 4.5 m. The holes are drilled with a diameter of 115 mm, an inclination of 5° to the vertical and the depth of the holes is 10 m.

The overdrilling depth is 1 m with a final head packing at 2 m. The line method is applied to the free face of the blast and the platform before the blast and allows the linear fracture density and fracture spacing to be calculated. It consists of defining a line that crosses the core front and platform and measuring all the fractures that intercept this line. This line must intercept the fractures present on the free face and platform and at a given length. Twelves 12 m long measurement lines were taken for each blasting, where the spacing and density of fractures and discontinuity planes were measured, allowing the calculation of parameters such linear density and average spacing between discontinuities.

Linear density and mean spacing between discontinuities are given by Porokhovoi's (1995) formula according to Eqs. (1) and (2).

$$D_1 = \frac{N}{l}, \tag{1}$$

D_l: linear fracture density (fracture/m); N: number of fractures intersected by the measurement line; l: length of measurement line (m).

$$E_m = d/n_d, \tag{2}$$

E_m: mean spacing between fractures (m); d: sum of distances between the successive fractures on a measurement line (m); n_d: number of distances between fractures.

The Rock Quality Designation (RQD) which is the first index for the evaluation of fracturing from core analysis is obtained by Eq. (3).

$$RQD = \left(\sum_{i=1}^{n} X_i/L \right) \times 100, \tag{3}$$

X_i: length of the ith segment free of fractures and greater than 0.1 m (m); L: total length d of the sampling line on which the RQD is calculated (m); n: number of fractures intersected by the measurement of the sampling line.

Discontinuities, mechanical properties and explosive consumption

Explosive consumption, on which the total energy reserve of the charge depends, is a factor that influences the quality of rock fragmentation (Ash 1973; Singh et al 2015).

The influence of discontinuities on the degree of fragmentation of a rock is characterized by the distance between cracks, their width and their place in the rock. Ash in 1973 developed an empirical formula between specific explosive consumption ($Q_{exp,\, Anfo}$ in Anfo (kg/m^3)), rock properties including fracture frequency and shear strength expressed in Eq. (4).

Table 2 shows the data for average fracture frequencies collected in the field and the resulting specific explosive consumption as a function of rock parameters, and allows Ash's curve to be plotted.

$$Q_{\exp, Anfo} = 1.4 \tan\left(\emptyset + i\right) / \sqrt[3]{\text{fracture/meter}}, \tag{4}$$

Table 1 Direction, dip, compressive strength and hardness index of blasting planes

Direction of blasting plane	N80E	N20E	N56E	N156E	N40E	N08E	N120E
Dip (°)	60°	70°	75°	82°	85°	86°	90°
Compressive strength (Mpa)	94.7	86.8	82.8	76.2	75	74	71
Hardness index (f)	9.47	8.68	8.28	7.62	7.5	7.4	7.1

Table 2 Specific consumption of explosive and frequency of fractures

Fracture/meter (m^{-1})	0.69	1.06	1.4	1.4	1.5	1.5	1.6	1.64	2.27
Specific consumption of explosive, Anfo (kg/m^3)	3.566	3.091	2.817	2.817	2.753	2.753	2.694	2.672	2.398

where ∅ is the angle of internal friction of the rock (°) Eq. (5) (M'zonchem and Chenafa 2006)

$$\varnothing = \arcsin\left(\left(R_c - 4R_t\right)/\left(R_c - 2R_t\right)\right), \tag{5}$$

and i the roughness angle of the fracture surfaces (°) Eq. (6) (Meftah 2010)

$$i = \varnothing/3, \tag{6}$$

R_c and R_t are the compressive and the tensile strength in (MPa), respectively.

Methods

The Kuz–Ram model is the most widely used approach to predicting rock fragmentation by blasting and has the advantage that it combines the rock properties of natural discontinuities and physical–mechanical characteristics, explosive properties and design variables (Cunningham 1983, 1987, 2005).

This model has three key equations, the Kuznetsov (1973) equation, the Rosin and Rammler (1933) equation and the Cunningham (1983, 1987, 2005) equation as shown in equations (Eqs. 7, 15, 16).

The fragment size for 50% of the material to pass through the crusher is given by Eq. (7) of Kuznetsov (1973).

$$X_m = A \times \left(\frac{V}{Q_e}\right)^{0.8} \times Q_e^{\,0.167}, \tag{7}$$

X_m: the mean size of blocks which 50% of passing materials through the crusher (cm); A: rock factor; V: volume of rock broken per blast hole (m^3); Q_e: mass of explosive in the blast hole (kg); K is the powder factor or specific charge (Eqs. 8 and 9) (Belhous 2016; Gadikor 2018; Segaetsho and Zvarivadza 2019).

$$K = Q_e/V, \tag{8}$$

$$K = q_{et} \times K_{ex} \times K_{fiss} \times K_d \times K_c \times K_v \times K_{sd}, \tag{9}$$

q_{et}: rock blastability (kg/m^3); q_{et}: blastability of the rock (kg/m^3); K_{ex}: transformation index of the standard explosive; K_{fiss}: cracked index which considering the cracking of the rock; K_d: index which considering the degree of fragmentation; K_c: index which considering the degree of real concentration of the load; K_v: index which considering the influence of the volume of blasted rock for the steps; K_{sd}: index which considering of the arrangement of the load and the surface number of the rock attracted by case in two free surfaces.

The blastability of the rock mass (q_{et}) makes it possible to characterize its class. It varies according to the mechanical properties of the rock and the dip of the planes of discontinuities. It is given by Eqs. (10), (11), (12) and (13) (Belhous 2016).

$$q_{et} = 0.02 \times \left(\sigma_c + \sigma_{tr} + \tau\right) + 2\rho, \tag{10}$$

$$\sigma_c = 100 \times f, \tag{11}$$

$$\sigma_{tr} = 0.33 \times \sigma_c, \tag{12}$$

$$\tau = \sigma_c/10, \tag{13}$$

σ_c: strength of the rock to simple compression (MPa); σ_{tr}: strength of the rock to traction (MPa); τ: strength of the rock to shear (MPa); ρ: density of the rock (kg/l); f: hardness index.

Cunningham (2005) stated that, the evaluation of the rock factor for blasting should at least take into account the density, mechanical strength, elastic properties and structure of the material (Table 3). The rock factor (A) is given by Eq. (14) (Gheibie et al. 2009; Mohammad et al. 2019):

$$A = 0.06 \times (\mathrm{RMD} + \mathrm{JF} + \mathrm{RDI} + \mathrm{HF}), \tag{14}$$

RMD: mass description; JF: joint factor; RDI: rock density influence; HF: hardness factor.

The Rosin–Rammler distribution (Rosin and Rammler 1933) used to evaluate the proportion of blocks passing through the crusher is given in Eq. (15).

$$P(X) = 100 \times \left(1 - \exp\left(-\left(\frac{X}{X_c}\right)^{ni}\right)\right) \tag{15}$$

$P(x)$: proportion of passing blocks in the crusher (%); ni: uniformity index; X_c: characteristic size of blocks which 63.2% of passing materials (cm); X: the blocks size (cm).

Equation (15) further established by Cunningham (1987) used to calculate the uniformity index (ni) by incorporating the effects of blast geometry is shown in Eq. (16).

Table 3 Rock factor parameters and rates (Mohammad et al. 2019)

Parameters	Sub-category	Rating
Rock mass description (RMD)	Powdery	10
	Vertically jointed	20
	Massive	50
Joint plane spacing (JPS)	< 0.1 m	10
	0.1 m to oversize	20
	Oversize to pattern size	50
Joint plane angle (JPA)	Horizontal dip	10
	Discontinuity dip out of face	20
	Discontinuity dip perpendicular to face	30
	Discontinuity dip into face	40
Rock density index (RDI)	Density (kg/l)	25–50
Hardness factor (HF)	If Ym < 50 GPa	UCS/3
	If Ym > 50 GPa	UCS/5

Ym Youg's modulus, *UCS* uniaxial compressive strength

$$ni = \left(2.2 - 14\left(\frac{B}{D}\right)\right) \times \left(1 - \left(\frac{W}{B}\right)\right) \times \left(\frac{\left(1 + \left(\frac{E}{B}\right)\right)}{2}\right)^{0.5} \times \left(\frac{L}{H}\right), \tag{16}$$

B: burden (m); E: spacing (m); D: blasthole diameter (mm); W: standard deviation of drilling (m); L: charge length (m); H = bench height (m).

Using Eq. (15) of Rosin and Rammler (1933), the characteristic size is calculated from the average size by substituting $X = X_m$, and $y = 0.5$ in Eq. (15) which gives Eq. (17).

$$X_c = X_m/(O.693)^{\frac{1}{ni}}, \tag{17}$$

X_m: the mean size of blocks which 50% of passing materials through the crusher (cm),

The standard deviation of drilling (W in meter) is given by Eq. (18) (Gaucher 2011).

$$W = \frac{D}{1000} + \left(0.03 \times L_t\right), \tag{18}$$

L_t: total length of the hole (m).

The total hole length (L_t) is given by Eqs. (19) and (20) (Gaucher 2011).

$$L_t = \frac{H}{cos\mu} + L_{s,} \tag{19}$$

$$L_s = 0.3 \times B_{th,} \tag{20}$$

L_s: overdrilling of hole (m); B_{th}: theoretical burden (m); μ: angle of inclination of the hole relative to the vertical (°). The theoretical burden (B_{th} in meter) formula is given by the empirical relationship of Langefors and Kihlstrom (1979) in Eqs. (21), (22) and (23).

$$B_{th} = 1.08 \times \sqrt{(L_f \times S)}/\left(C_{in} \times R_t \times \left(\frac{E}{B}\right)\right), \tag{21}$$

R_t: index of strength to blastability; C_{in}: stress factor; S: the energy index Eq. (22) and L_f: linear load (kg/m in Eq. 23).

$$S = Q/Q_{0,} \tag{22}$$

Q: explosive energy of Explus (MJ/kg); Q_0: explosive energy of Anfo (MJ/kg);

$$L_f = \pi \times d_e \times \left(\frac{\phi^2}{4}\right) \times K_{t,} \tag{23}$$

d_e: density of the explosive (Explus and Anfo) used (g/m^3); ϕ: diameter of the explosive (Explus and Anfo) used (mm); k_t: explosive settlement index.

Langefors and Kihlstrom (1973) established an empirical formula to calculate the maximum allowable burden ($B_{\max}$ in meter) as a function of the drilling diameter and other parameters, including rock strength, mesh ratio, and the inclination and type of explosive (Salmi and Sellers 2021) by the following equation (Eq. 24).

$$B_{\max} = (0.958 \times D) \times \sqrt{(\rho_c \times S_e)}/\left(C_b \times C_{LK} \times \left(\frac{E}{B}\right)\right), \tag{24}$$

ρ_c: density of the charge (kg/m^3); S_e: weight strength; C_b: factor indicating the constraining effect of the material surrounding an explosive charge; C_{Lk}: rock constant known as the Langefors and Kihlstrom's blastability factor (kg/m^3).

Results and discussion

Quality of the Bidzar rock

The simple compressive strength of Bidzar marble is 75 MPa reflecting that, it is a medium hard, class II, R4 grade rock (Porokhovoi 1995; Gadikor 2018). The RQD of the rock is 93% showing that, this marble is of excellent quality (RQD class 1). The rock factor is about 10.455, confirming that, the rock is hard and moderately fissured (Ouchterlony and Sanchidrian 2019). The average fracture spacing is 1.08 m and the average spacing between the planes of the discontinuities is 80.53 cm (Table 4) showing that, the discontinuities are spaced and that, the Bidzar rock is class ES2. The average fracture density is 1.02 m^{-1} and the average density of the discontinuity planes is 1.60 m^{-1} (Table 4), indicating that the Bidzar marble is of class ID2 and low discontinuity density. The average spacing between discontinuities in the Bidzar marble is greater than 0.5 m. Taking into account the Central Research Institute's (CRI) blastability classification, the Bidzar marble is category III, thus difficult to blast (Salmi and Sellers 2021). In the same order, the Protodyakonov's hardness index of the Bidzar marble is 7.5 showing that, the Bidzar rock is exactly the marble as this one is between 7 and 9, of class III, resistant, solid and hard, difficult to blast according to the Protodyakonov classification (Salmi and Sellers 2021). The compressive strength of Bidzar marble is 75 Mpa, so between 50 and 100 Mpa, the powder factor varies between 0.522 kg/m^3 and 0.658 kg/m^3, ranging between 0.5 kg/m^3 and 0.8 kg/m^3, translating that the marble of the Bidzar quarry is of medium hardness, which agrees with the classification of Mohamed and Shapiro (Salmi and Sellers 2021). Moreover, the spacing between the fractures varies between 0.5 and 1 m showing that, Bidzar marble is moderately cracked and belongs to the difficult blastability class according to Khanukaev's

Table 4 Geometric parameters of discontinuity in Bidzar quarry

Lines	Position (m)	Direction	Average space of discontinuities (m)	Average frequency of discontinuities (m^{-1})	Average space of fractures (m)	Average frequency of fractures (m^{-1})
L1	X: 0404075 Y: 1098460 Z: 420	N80W W–E	0.9429	1.5	0.75	1.5
L2	X: 0404104 Y: 1098425 Z: 420	N60W WNW–ESE	0.7923	1.4	1.11	1
L3	X: 0404139 Y: 1098411 Z: 426	N40E SW–NE	0.6732	1.64	0.79	1.36
L4	X: 0404153 Y: 1098362 Z: 423	N72W WSW–ENE	1.0565	1.06	1.64	0.67
L5	X: 0404165 Y: 1098305 Z: 425	N80E W–E	0.7348	1.5	1.17	0.93
L6	X: 0404144 Y: 1097822 Z: 457	N90W W–E	1.64	0.69	0.7	0.13
L7	X: 0404215 Y: 109784 Z: 439	N90E W–E	0.4080	2.64	0.52	2
L8	X: 04042173 Y: 1097932 Z: 432	N80E E–W	0.8488	1.4	1.25	0.87
L9	X: 0404270 Y: 1097984 Z: 432	N16E SSW–NNE	0.5027	2.09	1.83	0.64
L10	X: 0404270 Y: 1097972 Z: 440	N60W WNW–ESE	0.4702	2.27	0.92	1.18
L11	X: 0404239 Y: 1097817 Z: 428	N140W NE–SW	0.7888	1.42	1.2	0.92

classification (Salmi and Sellers 2021). The density of Bidzar marble is between 2750 kg/m^3 and 2900 kg/m^3, accommodating with the classification of Gokhale (Salmi and Sellers 2021).

Natural discontinuity planes

Figure 2 shows three families of natural discontinuities in the Bidzar quarry, the major directions (N30–40E, N40–50E, N160–170E), the secondary directions (N10–20E, N50–60E, N80–90E, N140–150E, N150–160E, N170–180E) and minority directions (N00–10E, N20–30E, N40–50E, N70–80E, N100–110E, N110–120E, N120–130E, N130–140E) with a dip of about 85°. This hierarchy of direction families corresponds to that described by Ndjeng (1998) and Wouatong et al. (2017), reflecting that the Bidzar rock is fractured, a fracturing acquired both naturally during the volcano-sedimentary process that prevailed in the Bidzar area and also artificially by the multiple blasting carried out over decades of exploitation. Figure 3a, b shows the concentration of discontinuity poles and major discontinuity planes on the stereonet in 2D and 3D. Figure 3c gives the hierarchy of the discontinuity planes on the directional rosette and Fig. 3d presents the frequency histogram of the discontinuity planes. To this end, Fig. 3b highlights three planes: plane N028E69 with a west dip direction, plane N066E86 with a NNW dip direction and plane N289E88 with a SSW dip direction. The west dipping planes of the quarry are shallower in dip than the other planes and therefore favourable for producing optimal fragmentation after shooting.

Influence of discontinuities on explosive consumption

Figure 4 shows the influence of discontinuities and mechanical properties on explosive consumption. The shape of the curve for the evolution of the specific explosive consumption in Anfo as a function of the fracture frequency is decreasing. This curve varies in the same direction as that of Ash (1973), Salmi and Sellers (2021) and shows that the consumption of explosive in Anfo decreases as the fracture frequency increases (Fig. 4). This is due to the fact that discontinuities generate a wave reflection resulting in a concentration of stresses in the fractured zone which act in conjunction with those created by the explosive charge, resulting in a decrease in explosive consumption and better fragmentation. Eqs. (2) and (3) give for the Bidzar marble: the angle of internal friction 49.54°; the angle of roughness 16.51°; the angle of friction of 66.05° showing that, the planes of discontinuity are not very rough and the internal friction is low.

Proposal of the blasting plane

Tables 5, 6 and 7 show that, discontinuity planes with a dip greater than 60° are difficult to blast while, those with a dip less than or equal to 60° are a little more difficult. With the exception of the 60° dip blasting plane which is very difficult to pull and equal to 0.32056 g/m^3, the discontinuity planes with a dip greater than or equal to 60° and a pull of less than or equal to 0. 32,056 kg/m^3 are subvertical to vertical planes, and can be used as blasting planes, whereas discontinuity planes with a dip of less than 60° and a blastability of more than 0.32056 kg/m^3 are subhorizontal to horizontal planes, and cannot be blasting planes. This result is consistent with the work of Worsey et al. (1981), who show that if the dip of the discontinuity planes is less than 60°, the blasting results will become poor. The blastability of the blasting planes increases with decreasing dip (Tables 5, 6 and 7). The dip of the rock quarry is about 85° and average blastability 0.2654 g/m^3. Furthermore, the blastability of blasting planes increases with the increase of the powder factor and the compressive strength of blasting planes (Tables 5, 6 and 7).

Fragmentation as a function of compressive strength and powder factor

Table 1 shows that the compressive strength is a function of the dip of the blasting planes and the hardness of the free face. The dip of the blasting planes and their hardness are two dependent parameters varying in opposite directions. Figure 5 shows the percentage of blocks passing through the primary crusher at Bidzar quarry as a function of the dips of the blasting planes 60°, 70°, 75°, 82°, 85°, 86°, 90° and at variable mesh sizes 3 × 3 m, 4 × 4 m, 4.5 × 4.5 m, and show that productivity varies between 60.08 and 71.78%. Tables 5, 6 and 7 show that the uniformity index varies between 1.209 and 1.238, in line with De Lile's (2012) requirement that it should be between 0.8 and 2.2. It is 1.238 for the 3 × 3 m drilling mesh, 1.209 for the 4 × 4 m drilling mesh and 1.183 with the 4.5 × 4.5 m drilling mesh, reflecting that the distribution of block size after the blast in the Bidzar quarry is uniform. The powder factor is between 0.522 kg/m^3 and 0.658 kg/m^3, which is comparable to that of igneous rocks according to Gadikor (2018), and corresponds to that where rock fragmentation is difficult, reflecting that, more explosive should be used during blasting to have an effective fragmentation. Also, the average block size decreases with increasing powder factor, which agrees with the studies of Gadikor (2018). Tables 5, 6 and 7 further show that, fragmentation increases with increasing powder factor, and so does explosive consumption. The blasting pattern that produces optimal fragmentation is the one with the highest powder factor independent of the drilling mesh in agreement with the work of (Blair 2015).

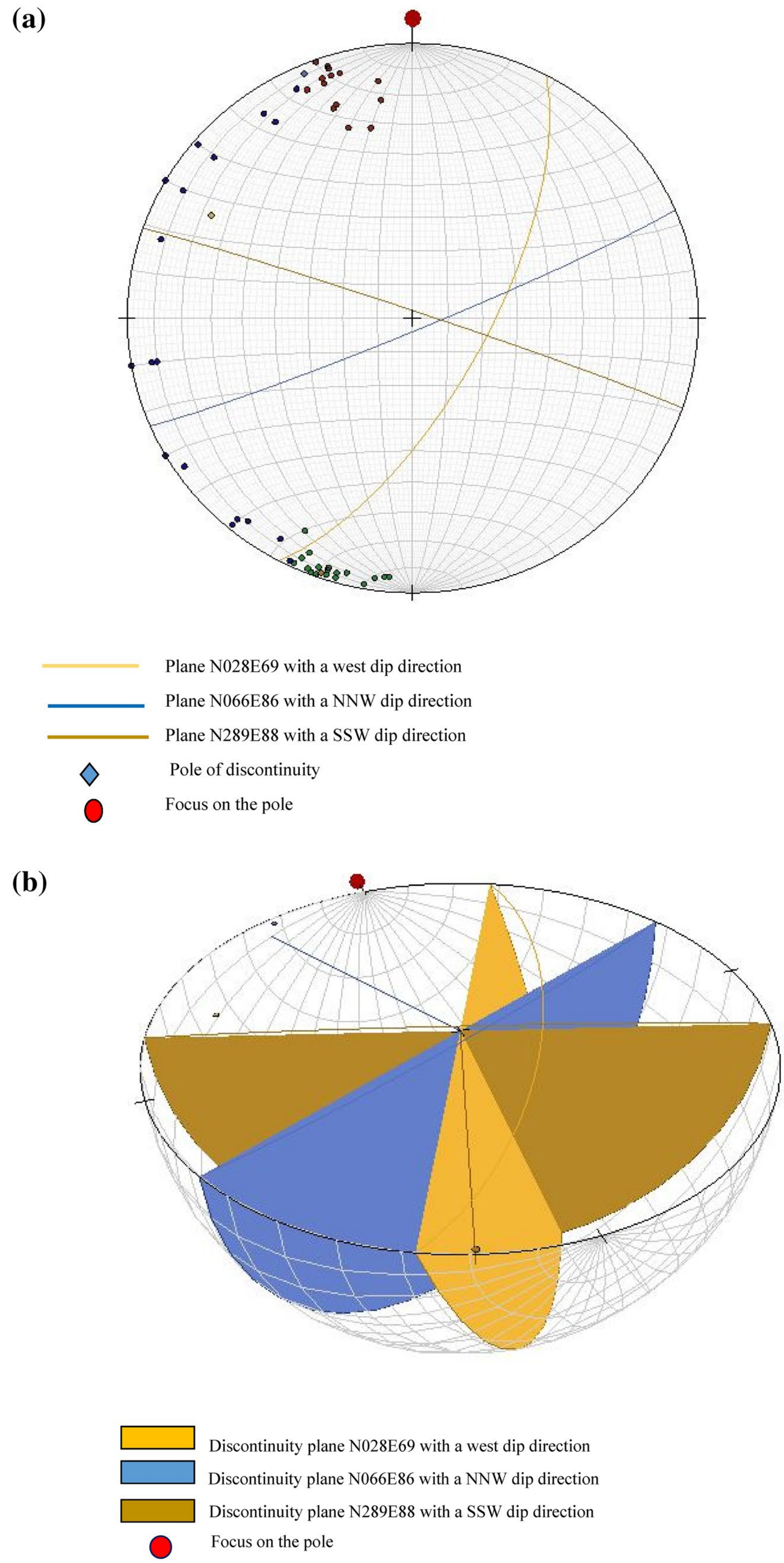

Fig. 3 Stereographic projection and major direction of discontinuity planes of the Bidzar quarry. **a** Stereographic projection of discontinuities. **b** Major discontinuity plane in 3D. **c** Major direction of discontinuity plane. **d** Frequency histogram of discontinuity planes

Fig. 3 (continued)

(c)

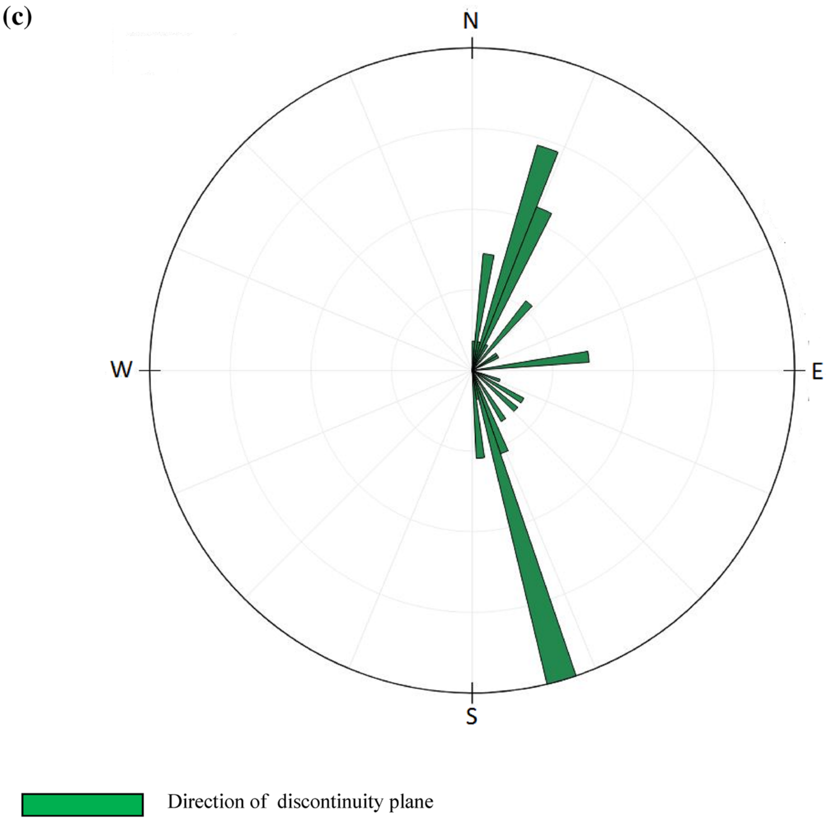

(d)

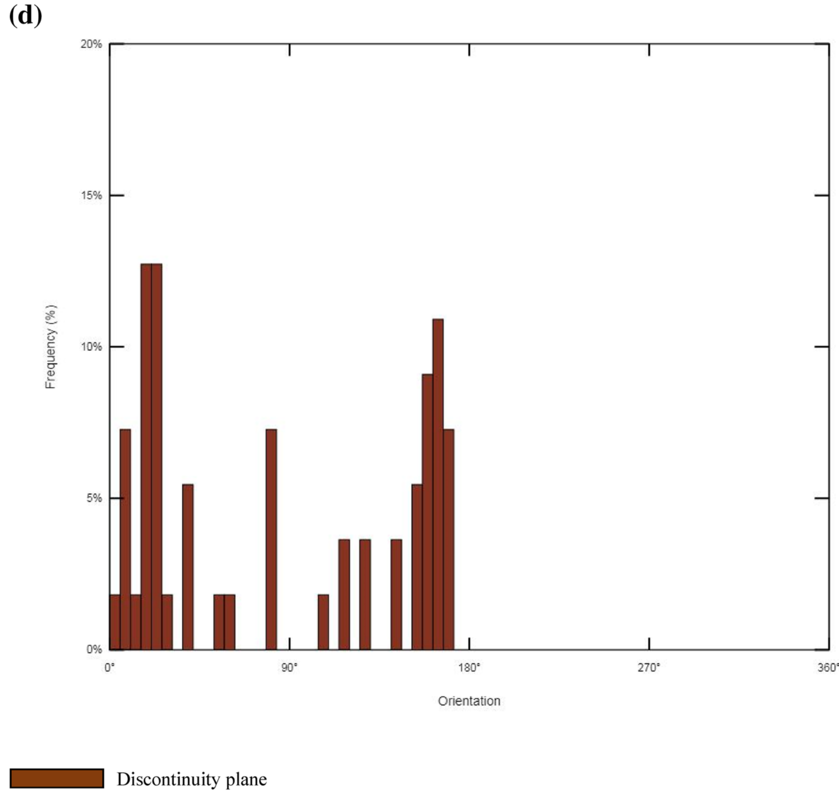

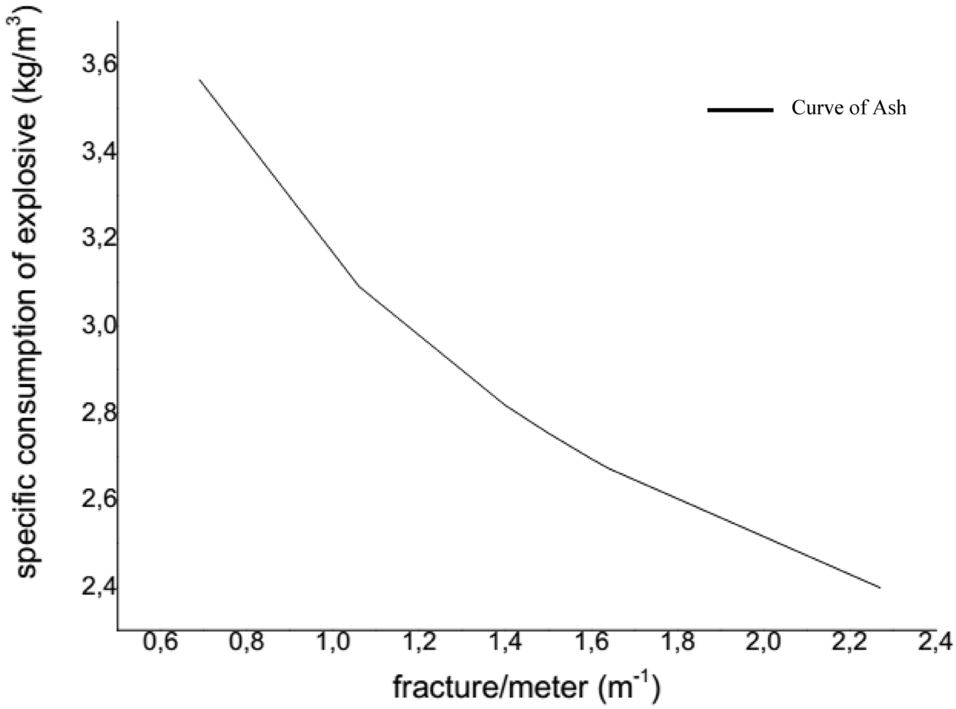

Fig. 4 Curve of explosive consumption function of the frequency of fractures and shear strength

Figure 6 shows that, as the compressive strength of the blasting planes increases, the powder factor increases, a result that is in agreement with the work of Muftuoglu et al. (1991). Indeed, increasing the compressive strength of the blasting planes increases the powder factor and the consumption of explosive which leads to an increase in fragmentation. These results are consistent with those of (Blair 2015; Salmi and Sellers 2021) who explain that high density rocks tend to require higher explosive energy to produce fragmentation than low density rocks. Tables 5, 6 and 7 show that dipping blasting planes (75°, 82°, 86°, 90°) have a compressive strength between 8 and 80 Mpa and correspond to semi-hard fronts, whereas dipping blasting planes (60°, 70°, 75°) have a compressive strength greater than 80 Mpa, indicating that they constitute hard fronts (Porokhovoi 1995). As a result, blasting planes with hard felling faces give a higher powder factor and generate the best fragmentation after shooting, which is the opposite for blasting planes with semi-hard faces. The 60° dip blasting plane with a maximum compressive strength of 94.7 Mpa, has a maximum powder factor of 0.658 kg/m^3, and produces optimum yields at different mesh sizes: 71.78% at 3 × 3 m, 67.85% at 4 × 4 m, 66.46% at 4.5 × 4.5 m. The simple compressive strength of the Bidzar rock is 75 Mpa and dips 85°, indicating that the marble is hard, resistant and therefore requires a high explosive energy for efficient fragmentation.

Fragmentation as a function of the dip of the blast planes and the drilling mesh

In the Bidzar quarry, the average size of the blasted blocks (Xm) should be between 150 and 550 mm, for a crusher jaw of 550 mm. Thus, blasting with the 3 × 3 m drilling mesh in the dip, 60°, 70°, 75°, 82°, 85°, 86°, and 90° blasting planes gives a Rosin–Rammler slope (X/Xc) greater than 1 showing a high level of fragmentation. In contrast, the blast with the 4 × 4 m and 4.5 × 4.5 m drilling mesh give Rosin–Rammler slopes (X/Xc) greater than 1 for dipping blasting planes (60°, 70°, 75°, 82°) and (60°, 70°, 75°) and less than 1 for dipping blasting planes (85°, 86°, 90°) and (82°, 85°, 86°, 90°), respectively. These results show that the Rosin–Rammler slope (X/Xc) increases with decreasing dip of the blasting planes and drilling mesh. The Rosin–Rammler slope allows not only to observe the variation of the Rosin–Rammler distribution curves but also to deduce the level of fragmentation. Figure 7 shows the Rosin–Rammler distribution curves or fragmentation curves and describes the size distribution of the fragments after the blast as a function of the dips of the blasting planes and the drilling mesh. For visibility of the fragmentation curves, the dip blasting planes (60°, 75°, 82°, 90°) were chosen. This choice is justified by the fact that the nearby dip and Rosin–Rammler slope blasting planes have almost identical Rosin–Rammler curves. These are the dipping blasting planes (82°, 85°, 86°) on the one

Table 5 Parameters of Kuz–Ram prediction model q_{et}, k, X/Xc, Q, Xm, *n*, Xc, P(x) with mesh size 3×3 m according to the dips and compressive strengths of the blasting planes

Direction of blasting planes	+− Dip (°)	Compressive strength (Mpa)	Spacing (m)	Burden (m)	W (m)	qet (kg/m^3)	K (kg/m^3)	X/Xc	Qe (kg)	Xm (cm)	*n*	Xc (cm)	P (X)%
N80E	60°	94.7	3	3	0.469	0.3205	0.658	1.209	59.25	28.88	1.238	45.475	71.78
N20E	70°	86.8	3	3	0.469	0.2984	0.612	1.155	55.161	30.217	1.238	47.581	69.77
N56E	75°	82.8	3	3	0.469	0.2872	0.589	1.282	53.091	30.953	1.238	48.747	68.68
N156E	82°	76.2	3	3	0.469	0.2718	0.558	1.089	50.245	32.057	1.238	50.477	67.11
N40E	85°	75	3	3	0.469	0.2654	0.545	1.067	49.054	32.547	1.238	51.249	66.42
N08E	86°	74	3	3	0.469	0.2626	0.539	1.066	48.537	32.766	1.238	51.594	66.11
N120E	90°	71	3	3	0.469	0.2542	0.522	1.044	46.984	33.448	1.238	52.667	65.18

Table 6 Parameters of Kuz–Ram prediction model q_{et}, k, X/Xc, Q, Xm, *n*, Xc, P(x) with mesh size 4 m×4 m according to the dip and compressive strengths of the blasting planes

Direction of blasting planes	Dip (°)	Compressive strength (Mpa)	Spacing (m)	Burden (m)	W (m)	qet (kg/m^3)	K (kg/m^3)	X/Xc	Qe (kg)	Xm (cm)	*n*	Xc (cm)	P (X)%
N80E	60°	94.7	4	4	0.469	0.3205	0.658	1.110	105.333	31.793	1.209	49.532	67.85
N20E	70°	86.8	4	4	0.469	0.2984	0.612	1.061	98.065	33.265	1.209	51.825	65.82
N56E	75°	82.8	4	4	0.469	0.2872	0.589	1.035	94.385	34.08	1.209	53.095	64.77
N156E	82°	76.2	4	4	0.469	0.2718	0.558	1.000	89.324	35.29	1.209	54.980	63.62
N40E	85°	75	4	4	0.469	0.2654	0.545	0.985	87.208	35.86	1.209	55.821	62.55
N08E	86°	74	4	4	0.469	0.2626	0.539	0.978	86.288	36.071	1.209	56.197	62.25
N120E	90°	71	4	4	0.469	0.2542	0.522	0.958	83.528	36.821	1.209	57.365	61.33

Table 7 Parameters of Kuz–Ram prediction model q_{et}, k, X/Xc, Q, Xm, *n*, Xc, P(x) with mesh size 4.5×4.5 m according to the dips and compressive strengths of the blasting planes

Direction of blasting planes	Dip (°)	Compressive strength (Mpa)	Spacing (m)	Burden (m)	W (m)	qet (kg/m^3)	K (kg/m^3)	X/Xc	Qe (kg)	Xm (cm)	*n*	Xc (cm)	P (X)
N80E	60°	94.7	4.5	4.5	0.469	0.3205	0.658	1.077	133.313	33.068	1.183	51.030	66.46
N20E	70°	86.8	4.5	4.5	0.469	0.2984	0.612	1.030	124.113	34.600	1.183	53.393	64.50
N56E	75°	82.8	4.5	4.5	0.469	0.2872	0.539	1.005	119.456	35.447	1.183	54.702	62.44
N156E	82°	76.2	4.5	4.5	0.469	0.2718	0.558	0.970	113.051	36.706	1.183	56.644	61.93
N40E	85°	75	4.5	4.5	0.469	0.2654	0.545	0.956	110.373	37.267	1.183	57.510	61.27
N08E	86°	74	4.5	4.5	0.469	0.2626	0.539	0.949	109.208	37.518	1.183	57.897	60.97
N120E	90°	71	4.5	4.5	0.469	0.2542	0.522	0.930	105.715	38.298	1.183	59.101	60.08

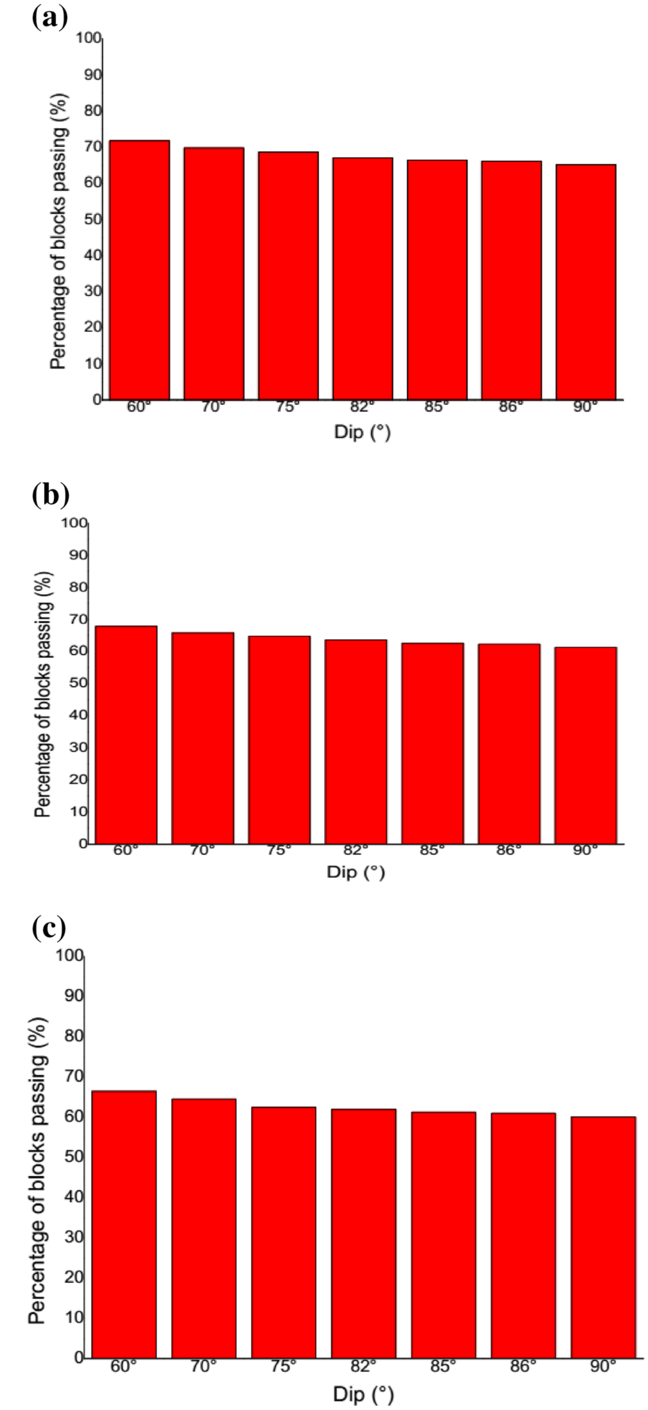

Fig. 5 Percentage of blocks passing to the crusher for blasting planes to the 60°, 70°,75°, 82°, 85°,86°, 90°, dip with mesh sizes 3 ×3 m, 4 ×4 m and 4.5×4.5 m. **A** Percentage of blocks passing to the crusher with mesh size 3×3 m. **B** Percentage of blocks passing to the crusher with mesh size 4×4 m. **C** Percentage of blocks passing to the crusher with mesh size 4.5×4.5 m

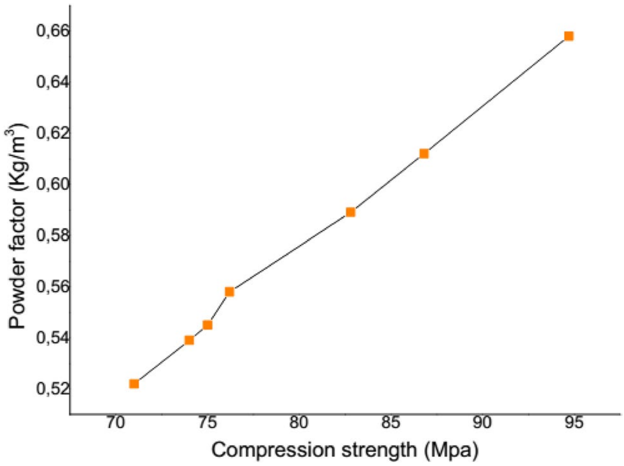

Fig. 6 Powder factor versus a rock compression strength

hand and the dipping planes of (70°, 75°) on the other. The dipping blasting planes (85°, 86°) have almost similar dips and Rosin–Rammler slopes and are closer to the 90° dipping blasting plane than the 82° dipping blasting plane (Tables 5, 6 and 7). The Rosin–Rammler slopes vary between 0.930 and 1.209 for the different blasting planes of dips: 60°, 70°, 75°, 82°, 85°, 86°, 90° and the drill holes 3 × 3 m, 4 × 4 m and 4.5 × 4.5 m. In this quarry, the blasting plane producing an optimal yield of blocks after the blast is the 60° dip discontinuity plane at the 3 × 3 m mesh, with a Rosin–Rammler slope of 1.209.

Furthermore, for the same borehole, the productivity of the blocks passing to the crusher increases as the dip of the blasting planes and the borehole mesh decreases and as the amount of explosive, the powder factor and the compressive strength increase. Finally, for the same borehole, the amount of explosive and the powder factor increase the borehole mesh and the compressive strength, respectively. The standard deviation of drilling varies with the borehole diameter and does not depend on the mesh size, and is 0.469 m. The maximum burden in the Bidzar marble quarry is 4.487 m and corresponds precisely to the one currently used. The real burden is 3.930 m, the theoretical burden is 4.339 m and the total borehole length is 11.357 m. The decrease in dip leads to an increase in the compressive strength of the blast plane and the hardness of the slope, resulting in an increase in the explosive load and the powder factor of the face to be blasted, thus reducing the average block size and increasing productivity (Tables 5, 6 and 7). These results are consistent with the work of Singh et al. (2015), regarding the decrease in block size with the reduction of the drilling mesh and, the work of Belland (1968), Worsey et al. (1981) and Yahyaoui et al. (2018) according to which the dip of the main parting planes significantly influences fragmentation. Tables 5, 6 and 7 and Fig. 7 clearly show that, the directions of the blasting planes do not influence the fragmentation of the rocks but rather, the dip of the blasting planes. This result is cited in the work of Belland (1968) and Yahyaoui et al. (2018). On the other hand, the directions of the blasting planes impact on stability, good front alignment and felling difficulties. A result that also agrees with those of Ash (1973) and Yahyaoui et al. (2018). In comparison with the results obtained by Shaib et al. (2020), Bidzar's model is reliable with 100% of the blocks passing the 250 cm size crusher screen.

Conclusion

The aim of this work was to enhance the geological and mechanical information of the Bidzar marble quarry and predict its fragmentation, considering the effect of its natural discontinuities and mechanical properties using the Kuz–Ram method. The prediction test was carried out with several blasting planes depending on the direction, dip and compressive strength. The influence of natural discontinuities and mechanical characteristics on the fragmentation of marble was thus studied. The remarkable results show that, the rock quarry is heterogeneous, consisting mainly of marble, with a dip of about 85°, fissured and hard, with a rock factor of 10.455, class III and difficult to blast. The marble from the Bidzar quarry is of excellent quality with an RQD of 93%. Fractures and discontinuity planes are spaced and of class ES2, the density of fractures and discontinuity planes is low and of class ID2. The rock quarry is intersected by a network of discontinuity planes marked by three families of direction, major (N30-40E, N40-50E, N160–170E), secondary (N10–20E, N50–60E, N80–90E, N140–150E, N150–160E, N170–180E) and minority (N00–10E, N20-30E, N40–50E, N70–80E, N100–110E, N110–120E, N120–130E, N130–140E). The percentage distribution of blocks passing through the primary crusher at Bidzar quarry according to the dips of the blasting planes 60°, 70°, 75°, 82°, 85°, 86°, 90° and at variable mesh sizes 3 × 3 m, 4 × 4 m, 4.5 × 4.5 m, varies between 60.08 and 71.78%. Furthermore, the discontinuity planes that can be considered as blasting planes are those with difficult to very difficult blastability and whose dips are between 60° and 90°, with the optimum plane being the 60° dip. Fragmentation increases inversely with the dip of the blasting planes. Finally, fragmentation decreases with the increase in the drilling mesh and the hard blasting planes with compressive strengths greater than 90 Mpa produce the best fragments.

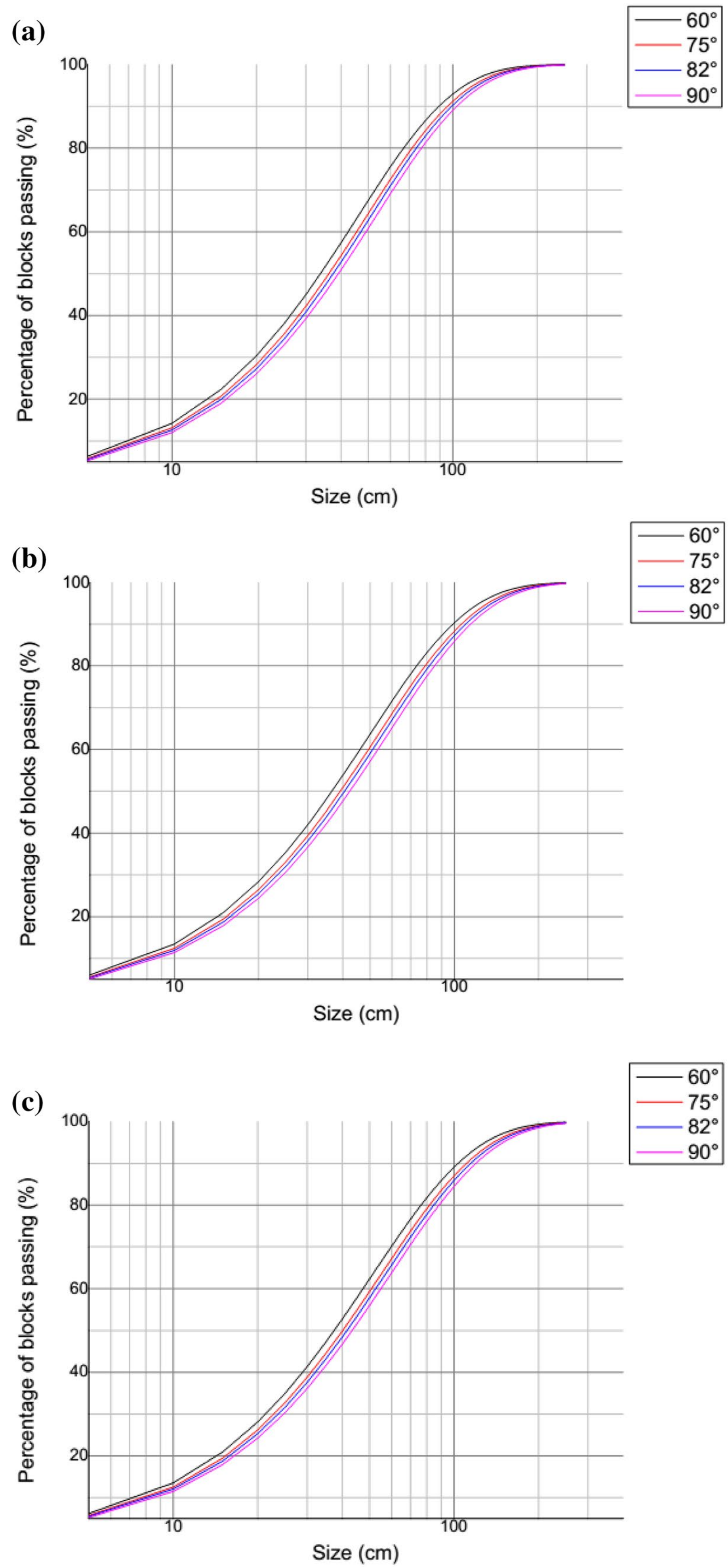

Fig. 7 Rosin–Rammler distribution curve following the blasting planes to the 60°, 75°,82°, 90° dip with mesh sizes 3×3 m, 4 ×4 m and 4.5×4.5 m. (i). Rosin–Rammler distribution curve with mesh size 3×3 m. (ii). Rosin–Rammler distribution curve following the blasting planes to the 60°,75°,82°, 90°dip with mesh size 4×4 m. (iii). Rosin–Rammler distribution curve with mesh size 4.5×4.5 m

Acknowledgements The authors thank the Director of CIMENCAM-Figuil, for his field assistance as well as the head of the laboratory for the physical and mechanical tests and the head of quarry service of CIMENCAM-Figuil. We would like to thank especially Editor-in-Chief and his staff, for the publication facilities. We also appreciate the contribution of the anonymous reviewers and correction as well as.

Declarations

Conflict of interest Authors have declared that no competing interests exist.

References

Akbari M, Lashkaripour G, Yarahamdi BA, Ghafoori M (2015) Blastability evaluation for rock mass fragmentation in Iran central iron ore mines. Int J Min Sci Technol 25:59–66. https://doi.org/10.1016/j.ijmst.2014.11.008

Ash RL (1973) The influence of geological discontinuities on rock blasting, Ph.D. Thesis, University of Missouri Rolla 87

Belhous M (2016) Elaboration d'un plan de tir pour améliorer la fragmentation des roches -Cas de la carrière d'Ain El Kebira, Université Abderrahmane Mira de Bejaia, Faculté de Technologie, Département des mines et géologie, mémoire en vue de l'obtention du diplôme de master en mines option exploitation minière

Belland JM (1968) Structure as a control in rock fragmentation coal lake iron ore deposited. The Canadian Mining Metallurgical Bull 59(647):323–328

Blair AC (2015) A novel powder factor based bench blast design method for large surface coalmines. Doctoral dissertations, Missouri University of Science and Technology

Burkle WC (1979) Geology and its effect on blasting. In: Proceedings of the 5th conference on explosives and blasting techniques, SEE

Cho SH, Katsuhiko K (2004) Rock fragmentation control in blasting. Mining Mater Process Inst Japan, Mater Trans 45(5):1722–1730

Cruise J (2011) Rock breaking—a science, not an art. Southern African Institute of Mining and Metallurgy, Namibia

Cunningham CV (1983) The Kuz-Ram model for the prediction of fragmentation from blasting, proceedings of the international symposium on rock fragmentation and blasting, Lulea, August 22–26

Cunningham CV (1987) Fragmentation estimations and the Kuz-Ram model-four years on, proceedings of the second international symposium on rock fragmentation by blasting, Keystone, August 23–26

Cunningham CV (2005) The Kuz-Ram fragmentation model-20 years on, 2005. In: European federation of explosives engineers, Brighton conference proceeding. Brighton, UK, pp 201–210

De Lile F (2012) Recherche d'une prédiction de fragmentation charge par charge pour les tirs à ciel ouvert, Ecole des mines de Paris, Thèse de Doctorat

Ebrahimi E, Monjezi M, Khalesi MR, Armaghani DJ (2015) Prediction and optimization of back-break and rock fragmentation using an artificial neural network and a bee colony algorithm. Bull Eng Geol Environ, Springer-Verlag Berlin Heidelberg, pp 1–10. http://doi.org//https://doi.org/10.1007/s10064-015-0720-2

Gadikor J (2018) Optimization of drilling and blasting practices at a Western US open pit copper mine. Graduate Theses and Non-Theses. 168, Master of Science in Mining Engineering Montana Tech

Gaucher F (2011). Planification des travaux de sautage excavation par bancs à ciel ouvert d'une carrière de calcaire fossilifère. Goldman Exploration, 860 boul. de la Chaudière Québec, Qc, G1X 4B7Le 31 octobre 2011

Gheibie S, Aghababaei H, Hoseinie SH, Pourrahimian Y (2009) Modified Kuz-Ram fragmentation model and its use at the Sungun copper Mine. Int J Rock Mech Min Sci 46(2009):967–973

Huang J, Asteris PG, Pasha SMK, Ahmed Salih Mohammed AS, Hasanipanah M (2020) A newauto-tuning model for predicting the rock fragmentation: a cat swarm optimization algorithm. Engineering with Computers, Springer-Verlag London Ltd., part of Springer Nature, pp 1–12. https://doi.org/10.1007/s00366-020-01207-4

Hustrulid W (1999) Blasting principles for open pit mining, vol 1. A.A. Balkema Pub

Jug J, Stjepan S, Gazdek M, Kavur B (2017) Fragment size distribution of blasted rock mass. World multidisciplinary earth sciences symposium (WMESS 2017) IOP publishing, OP Conf. Series: Earth and Environmental Science 95 042013, pp 1–2

Kuznetsov VM (1973) The mean diameter of fragments formed by blasting rock. J Min Sci 9:144–148

Langefors U, Kihlstrom B (1973) The modern technique of rock blasting. John Wiley & Sons, New York, London, Sydney, Toronto

Langefors U, Kihlstrom B (1979) The modern technique of rock blasting, AWE/Gebers, Stockholms, Suede

M'zonchem K and Chenafa W (2006) Etude géotechnique de la stabilité des talus dans la carrière de Ain El Kebira. Mémoire de finn d'étude du diplôme d'ingénieur d'état en géologie, Université de Sétif

Meftah A (2010) Méthode de soutènements des écrans de soutènements, chapitre 2

Mohammad B, Mohammad A, Farhang S, Farzad S, Sadjad M (2019) A new framework for evaluation of rock fragmentation in open pit mines. Faculty of mining engineering, petroleum and geophysics, Shahrood University of technology, Shahrood, Iran. J Mech Geotech Eng 11:325–336

Muftuoglu Y, Amehmetoglu A, Karpuz C (1991) Correlation of powder factor with physical rock properties and rotary drill performance in Turkish surface coal mines. In: Wittke, W. (Ed.), The 7th ISRM Congress. International Society for Rock. Mechanics, Aachen, Germany

Ndjeng E (1998) Sedimentary structures of the Babouri-Figuil basin (Bénoué ditch) in North Cameroon. In geoscience of Cameroon as Vicat J and Bilong P, collect GEOCAM 1/1998, Press University of Yaounde I

Ouchterlony F, Sanchidrián JA (2019) Review of development of better prediction equations for blast fragmentation. J Rock Mech Geotech Eng 11:1094–1109

Porokhovoï E (1995) Stabilité à long terme des talus de mines à ciel ouvert dans les massifs de roches basiques et ultrabasiques, Thèse de Doctorat, Ecole nationale des ponts et chaussées en géologie de l'ingénieur

Rosin P, Rammler E (1933) The laws governing the fineness of powdered coal. J Inst Fuel 7:29–36

Salmi EF, Sellers EJ (2021) A review of the methods to incorporate the geological and geotechnical characteristics of rock masses in blastability assessments for selective blast design. Eng Geol 281:105970

Segaetsho GSK (2017) Application of rock mass classification and blastability index for the improvement of wall control at Phoenix Mine, Faculty of Engineering and the Built Environment, University of the Witwatersrand, Johannesburg, in partial fulfilment of the requirements for the degree of Master of Science in Engineering, Johannesbourg

Segaetsho G, Zvarivadza T (2019) Application of rock mass classification and blastability index for the improvement of wall control: a hard rock mining case study 119: 1–40. http://doi.org/https://doi.org/10.17159/2411-9717/2019/v119n1a4

Shaib AS, Kudirat OY, Hashim MHM (2020) Comparative study of WipFrag image analysis and Kuz-Ram empirical model in granite aggregate quarry and their application for blast fragmentation rating, geomechanics and geoengineering, pp 1–10. http://doi.org/https://doi.org/10.1080/17486025.2020.1720830

Singh PK, Roy MP, Paswan RK, Sarim MD, Suraj K, Rakesh RJ (2015) Rock fragmentation control in open cast blasting. J Rock Mech Geotech Eng 8(2):225–237

Wouatong A, Kenmoe O, Ngapgue F, Katte V, Kamgang V (2017) A geological and physico-mechanical characterization of marble of the Bidzar quarry North-Cameroon. Br J Appl Sci Technol 19(5):2–7

Worsey PN, Farmer IW, Matheson GD (1981) The mechanics of pre-splitting in discontinuous rock. In: Proceedings 22nd US rock mechanics symp. University of Missouri Rolla, USA

Yahyaoui SA Hafsaoui A, Aissi A, Benselhoub A (2018) Relationship of the discontinuities and the rock blasting results. Dniprop, univer, bulletin, geology, geography

Yusong M, Yiping Z, Di u, Kebin L, Xianrong Y, Jie L (2021) Rock fragmentation size distribution prediction and blasting parameter optimization based on the Muck-Pile Model. Mining, Metallurgy & Exploration, Society for Mining, Metallurgy & Exploration Inc. 2021, Springer, pp 1–10. https://doi.org/10.1007/s42461-021-00384-0

Zhendong L, Yong F, Qidong G, Yingguo H (2020) Evaluation and optimization of blasting approaches to reducing oversize boulders and toes in open-pit mine. Int J Mining Sci Technol 30(3):373–380